Alteration of P450 Distal Pocket Solvent Leads to Impaired Proton Delivery and Changes in Heme Geometry†

Thomas M. Makris,‡ Konstanze von Koenig,§ Ilme Schlichting,§ and Stephen G. Sligar*,‡,||

Departments of Biochemistry and Chemistry and the School of Medicine, University of Illinois Urbana−Champaign, Urbana, Illinois 61801, and Max-Planck-Institut für medizinische Forschung, Abt. Biomolekulare Mechanismen, Jahnstrasse 29, 69120 Heidelberg, Germany

Received July 11, 2007; Revised Manuscript Received September 22, 2007

ABSTRACT: Distal pocket water molecules have been widely implicated in the delivery of protons required in O−O bond heterolysis in the P450 reaction cycle. Targeted dehydration of the cytochrome P450cam (CYP101) distal pocket through mutagenesis of a distal pocket glycine to either valine or threonine results in the alteration of spin state equilibria, and has dramatic consequences on the catalytic rate, coupling efficiency, and kinetic solvent isotope effect parameters, highlighting an important role of the active-site hydration level on P450 catalysis. Cryoradiolysis of the mutant CYP101 oxyferrous complexes further indicates a specific perturbation of proton-transfer events required for the transformation of ferric-peroxo to ferric-hydroperoxo states. Finally, crystallography of the 248Val and 248Thr mutants in both the ferric camphor bound resting state and ferric−cyano adducts shows both the alteration of hydrogen-bonding networks and the alteration of heme geometry parameters. Taken together, these results indicate that the distal pocket microenvironment governs the transformation of reactive heme-oxygen intermediates in P450 cytochromes.

The P450 cytochromes are a ubiquitous family of monooxygenases which utilize a thiolate ligated ferriheme cofactor to metabolize substrates of varying size and chemical functionality (*1*, *2*). While the molecular recognition events that dictate P450 substrate specificity have been described as "specialist" or "generalist" (*3*), according to a particular P450's metabolic role in varied anabolic and catabolic pathways, the P450s likely use a common reaction mechanism which employs the reductive cleavage of dioxygen to form a putative high-valent oxoferryl (the so-called compound I species (Figure 1)). In order to facilitate heterolytic scission of the O−O bond, the P450 enzyme must precisely control the delivery of an electron and two protons following formation of the metastable oxygen bound intermediate, the last kinetically observable species in the reaction cycle (*4*). Aberrations in proton-transfer events, which likely predominate in the reactions catalyzed by many P450 cytochromes, including those involved in drug detoxification, can also be observed in normally highly coupled P450s (e.g., CYP101[1] or P450cam) upon substrate alteration (*5*, *6*), or active-site mutagenesis (*7*, *8*). The net result is not only the nonproductive consumption of reducing equivalents but also generation of superoxide or hydrogen peroxide, resulting from the decay of oxyferrous (*9*), and one electron reduced hydroperoxo−ferric intermediates (*10*, *11*), respectively.

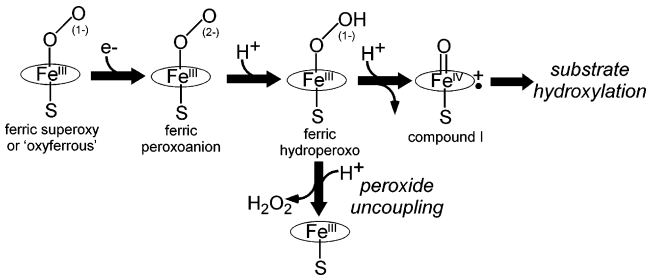

FIGURE 1: The oxygen activation pathway of P450 cytochromes, including sources of uncoupling to hydrogen peroxide formation.

The participation of the P450 active-site residues and sequestered water molecules in P450 proton mediated oxygen activation, and uncoupling pathways, has been extensively speculated upon since the original structure determination of CYP101 by Poulos (*12*), and has also been gauged against other heme (and non-heme iron) enzymes which employ a common set of chemical intermediates yet perform quite different chemistries, such as peroxidases and heme oxygenases. While subtle distinctions in the supply of protons, as mediated by the different active sites of peroxidases and P450s, have been briefly addressed in the comparison of peroxoferric intermediate generation and decay between oxygen activating heme enzyme classes (*13*, *14*), the pathway of proton delivery in the P450 active site remains an active

† This work was supported by a merit award from the National Institutes of Health (R37 GM31756) to S.G.S.

* To whom correspondence should be addressed. Telephone: (217) 244-7395. Fax: (217) 265-4073. E-mail: s-sligar@uiuc.edu.

‡ Department of Biochemistry, University of Illinois Urbana−Champaign.

§ Max-Planck-Institut für medizinische Forschung.

|| Department of Chemistry and the School of Medicine, University of Illinois Urbana−Champaign.

[1] Abbreviations: P450 or CYP, cytochrome P450 monooxygenase; CYP101 or P450cam, camphor 5-monooxygenase; EPR, electron paramagnetic resonance; KSIE, kinetic solvent isotope effect; ENDOR, electron nuclear double resonance; F_o, observed structure factor; F_c, calculated structure factor; NSD, normal-coordinate structural decomposition.

10.1021/bi7013695 CCC: $37.00
Published on Web 11/15/2007

area of study, due to its fundamental role in dictating a number of turnover parameters, including the release of reactive oxygen species generated at the expense of effective substrate oxygenation.

The roles of a conserved active site acid/alcohol pair have been addressed in a number of mutagenesis, spectroscopic, and structural studies (*7*, *8*, *10*, *11*, *15*−*20*). The accumulated data have indicated that substitution of the conserved acid residue (Asp251 in CYP101) results in impairment of oxyferrous reduction and subsequent proton-transfer processes, resulting in a slow enzyme which still catalyzes the monooxygenation reaction (*10*, *16*, *20*). Alteration of the conserved threonine, in contrast, results in an enzyme in which the electron and first proton transfer proceed normally, although the reaction coordinate instead favors the production of hydrogen peroxide rather than monooxygenation (*7*, *8*), due to an impairment of second proton delivery required for heterolytic O−O bond cleavage. While a wealth of studies have addressed the role of these two residues, including the structural determination of wild-type and mutant P450s in both the resting (*15*, *20*) and catalytically active oxyferrous states (*18*, *19*), the role of the remainder of the P450 distal pocket (including solvent) has lacked detailed mechanistic investigation. Given a high degree of structural conservation in P450 cytochromes, understanding the role of active-site residues and sequestered solvent in mediating effective oxygen activation chemistry may have important applications toward protein redesign, and has extensions to the mechanisms of a number of heme and non-heme metalloenzymes.

In order to probe the role of active-site hydrogen-bonding patterns and solvent on P450 catalysis, we have utilized a molecular dehydration approach, in which a series of bulky residues are introduced at a targeted position in the distal pocket and the ensuing kinetic and structural ramifications examined. Given the proximity of the Gly248 residue to the dioxygen moiety of oxyferrous CYP101 and surrounding solvent, this served as a logical choice for targeted dehydration of the P450 distal pocket. The Gly248 residue, which serves as a hydrogen bond partner with the side chain of Thr252 and results in an I-helix kink, is almost exclusively conserved as a small residue (Gly or Ala), and is in close proximity to the heme-bound dioxygen complex (*18*, *19*). One notable exception to this sequence conservation is in the mammalian CYP4 family, in which a glutamate participates in an autocatalytic post-translational modification, resulting in the transformation from a hexacoordinate heme resting state to an esterified heme adduct (*21*−*23*). Given the level of proximity to coordinated dioxygen and nearby active-site solvent (*18*, *19*), and the fact that the introduction of a carboxylate residue at this position results in a hexacoordinate ferriheme resting state in both CYP101 (*24*) and CYP102 (*25*), this site was chosen as an ideal candidate to explore the consequences of functional alteration of the heme distal pocket on P450 structure and catalysis. In this study, through a combination of site-directed mutagenesis, spectroscopy, kinetics, solvent-isotope effect and structural studies of two Gly248 variants (Gly248Thr and Gly248Val), we examine in detail the ramifications of active-site hydration on the oxygen activation mechanism of CYP101.

MATERIALS AND METHODS

Mutagenesis and Recombinant Expression of Wild-Type and Mutant P450s. Mutagenesis of the CYP101 gene (pCamT7) utilized the Stratagene Quikchange kit, according to methods developed by the manufacturer. All mutations were confirmed through sequencing of the entire CYP101 gene (ACGT, Wheeling, IL). The C-terminal 6x-His tagged CYP101 gene (pT7-P450 His) was expressed in BL21 (DE3) cells (Stratagene). Cells were grown in terrific broth at 37 °C, and induced with 1 mM IPTG at an OD of 0.8 and subsequently grown overnight in the presence of 0.5 mM δ-aminelavulinic acid to facilitate holoenzyme production. Cells were harvested by centrifugation and resuspended in 50 mM KPi pH 7.4, 150 mM KCl (buffer A), sonicated and spun by ultracentrifugation. A two-step purification protocol resulted in effective purification of CYP101-His (as judged both spectroscopically ($A_{391}/A_{280} > 1.45$) and via SDS−PAGE). First, the protein extract was loaded on a Ni-NTA column (Amersham), washed with buffer A in the presence of 50 mM imidazole, and eluted with buffer A supplemented with 20 mM EDTA. The resulting red fractions were dialyzed in 50 mM KPi, 400 μM D-camphor, 20 mM β-mercaptoethanol, pH 7.4 (designated as RB buffer) overnight at 4 °C. Solid ammonium sulfate was added to 30% saturation over 30 min and the protein was subsequently loaded onto a Phenyl-Sepharose CL6B column equilibrated in the same buffer, and eluted in a linear gradient from 30% to 0% ammonium sulfate. Resulting fractions with an Rz-value (A_{391}/A_{280}) greater than 1.45 were judged as pure and concentrated using an Amicon cell. The 6x-His tagged P450 construct showed identical spectroscopic and kinetic parameters to that of the non-His tagged construct expressed in *Escherichia coli*, and the native enzyme as expressed in *Pseudomonas putida*. All other components of the reconstituted system were expressed in *E. coli* and purified to homogeneity using previously published procedures (*16*) .

Spectroscopic Characterization of P450 Enzymes. Optical characterization was performed on a Cary 300 spectrophotometer (Varian). All spectra shown are in the presence of 200 μM D-camphor unless otherwise indicated. Electron paramagnetic resonance (EPR) spectra were obtained at the University of Illinois EPR Resource Center on a Varian E-122 X-Band (9.08 GHz) spectrometer, with a protein concentration of approximately 0.3 mM. EPR spectra of P450 variants in both the ferric resting state and the cryoradiolytically prepared peroxoferric state were collected at 20 K with a microwave power of 0.5 mW and modulation amplitude of 12.5 G at 100 kHz. A liquid helium flow system (Air Products, Allentown, PA) was used for measurements.

Steady-State Kinetics Assays. NADH oxidation assays were done according to protocols established earlier (*16*, *20*) using the following enzyme concentrations (0.5 μM P450, 1.1 μM putidaredoxin reductase, 5 μM putidaredoxin). Detection of hydroxycamphor was done via methods previously described (*20*) although a DB1 Megabore column (Agilent) was utilized with the following oven conditions: 80 °C isothermal, 5 min, followed by a temperature ramp of 5 °C/min to a final temperature of 150 °C. The amount of D-camphor (substrate) and 5-hydroxycamphor were calibrated using 3-bromocamphor as an internal standard.

Autoxidation of oxyferrous P450 was monitored by the decrease in absorbance at 418 nm at 25 °C.

Kinetic Solvent Isotope Effect (KSIE) Studies. Kinetic solvent isotope effects were measured using the methods described earlier (*20*), with a final percentage of D_2O calculated as being over 96% following exchange of P450 and associated redox partners by repeated concentration and dilution using Microcon concentrators (Amersham). In order to facilitate complete exchange, the proteins were incubated in deuterated solvent for at least 45 min prior to turnover experiments. The p*L* of all buffers was standardized at p*L* = 7.4 for all kinetics assays. For the comparison of coupling efficiencies in protium and deuterium containing solvents, 25 nmol of NADH was allowed to react to completion, as judged spectroscopically by decrease of NADH absorbance at 340 nm ($\epsilon = 6.22$ nmol^{-1} cm^{-1}). The organic products were extracted in chloroform and analyzed via the gas chromatographic analysis described above.

Generation of Peroxoferric P450 Complexes. Oxyferrous P450 was prepared by oxygenation of approximately 300 μM ferrous enzyme with oxygen at 4 °C as described in detail in earlier studies (*10*, *13*), although a pH of 7.4 was used. The frozen oxyferrous samples were irradiated with ^{60}Co at the Notre Dame Radiation Laboratory with a final accumulated dose of 4 Mrad and stored at 77 K until EPR data collection. Previous studies have indicated that while initial proton transfer (i.e., protonation of the peroxoanion to hydroperoxo species) can occur in wild-type P450 (*10*, *11*), the cryogenically prepared hydroperoxo species is stable for months at 77 K.

Crystallization and Preparation of the P450cam Cyanide Complexes. All mutants of P450cam were crystallized as described previously (*19*). The Gly248Thr mutant protein yielded rodlike crystals of spacegroup $P2_12_12_1$, whereas the Gly248Val mutant solely crystallized in bipyramidal crystals of spacegroup $P4_32_12$. Since this crystal form is unsuitable for oxygen complex preparation, both crystal forms were treated with potassium cyanide to yield a ligand complex that serves as a structural analogue of the P450 oxyferrous intermediate (*26*). Diffraction data were collected at the SLS beamline X10SA and reduced with the XDS program package (*27*). After an initial rigid body refinement step with CNS (*28*) using the protein moiety of the wild-type structure as a starting model (pdb codes 1akd and 1yrc for the orthorombic and tetragonal crystal forms, respectively), refinement was performed including simulated annealing and individual *B*-factor refinement steps. Potassium ions, camphor, and cyanide were added to the model in several rounds of manual rebuilding and refinement using CNS (*28*) or REFMAC (*29*). Default values for restraints, weights and water molecule assignment were used. Data collection and refinement statistics are summarized in Table 1. The coordinates and associated structure factors have been deposited with the Protein Data Bank (accession codes: Gly248Thr resting state, 2QBL, Gly248Thr−cyanide complex, 2QBM, Gly248Val resting state, 2QBN, Gly248Val cyanide complex, 2QBO). Figures displaying structures were generated with PyMOL (*30*). The superposition of structures was performed using Lsqkab (CCP4 suite) (*31*) using the entire P450 molecule with the exception of the I-helix.

RESULTS

Spectroscopic Characterization of Mutant P450 Enzymes

Optical spectroscopic characterization of the ferric camphor-bound, ferrous, and ferrous carbonmonoxy bound forms of 248Val and 248Thr (Figure 2) indicate features typical of P450 cytochromes and are virtually identical to spectroscopic parameters of wild-type CYP101. In particular, the introduction of either threonine or valine at the Gly248 position does not alter the high-spin conversion of P450 upon the binding of camphor, nor result in any perturbation of the carbonmonoxy bound ferrous form at 450 nm. This ensures that, despite the introduction of sterically larger groups in the distal pocket, both features of the proximal pocket, specifically thiolate ligation to the heme-iron, and binding of a gaseous diatomic ligand, are preserved.

In contrast, electron paramagnetic resonance (EPR) spectroscopy reveals distinguishable electronic changes at the P450 heme-iron in the Gly248 mutant enzymes (Figure 3). In comparison to the EPR spectrum of the wild-type camphor bound enzyme, which shows an approximately equal proportion of high- and low-spin species at 15 K, owing to a temperature-dependent spin equilibrium well-characterized earlier (*32*, *33*), the Gly248Thr and Gly248Val mutants show an almost exclusive high-spin species at low temperature. The increased high-spin fraction at low temperature is indicative of displacement of the coordinated axial-water in the distal pocket, resulting in an enzyme which, even at low temperature, is almost exclusively high-spin. In addition, the EPR *g*-values, in particular those of the predominant high-spin fraction (Table 2), demonstrate an increase of rhombicity of the heme-iron. The degree of rhombicity of high-spin iron has been shown earlier to vary among thiolate ligated ferriheme enzymes, and similar changes have been observed as a result of mutation of the conserved threonine to an alanine in CYP2B4 (*34*), and the binding of substrates to nitric oxide synthase (*35*), indicating that the microenvironment of the distal pocket may have an influence on the electronic parameters of the heme-iron, as is the case here. In this study, the electronic changes induced by Gly248 mutation can be directly attributed to a specific perturbation of heme geometry that results in an increase of porphyrin planarity, as discussed in further sections describing the crystal structures of the Gly248Thr and Val mutants in the camphor bound state.

Steady-State Kinetics of G248 Mutants

The steady-state kinetic profiles of the Gly248 mutants, in comparison to wild-type CYP101, are presented in Table 3. In agreement with previous studies which have shown that the distal pocket environment is critical in the delivery of protons to the ferric−peroxo and hydroperoxo complex necessary for cleaving the O−O bond, the introduction of a bulky residue at the 248 position is shown to elicit dramatic catalytic consequences. First, both the rates of overall electron consumption and hydroxycamphor formation decrease with an increase of steric restraint at the position. As a result of the valine substitution, the rate of hydroxycamphor formation is comparable to those of the well-characterized mutant of the alcohol pair, Asp251Asn, which has been shown earlier to result from a specific perturbation of second electron transfer and delivery of the first proton required for dioxygen

Table 1: Crystal Parameters, Data Collection, and Refinement Statistics

	Gly248Thr		Gly248Val	
protein complex	ferric	cyano	ferric	cyano
PDB code	2QBL	2QBM	2QBN	2QBO
space group	$P2_12_12_1$	$P2_12_12_1$	$P4_32_12$	$P4_32_12$
unit cell (*a*, *b*, *c*) [Å]	64.1, 64.6, 106.3	63.8, 64.6, 105.5	63.9, 63.9, 242.1	63.7, 63.7, 241.3
		Data Collection		
wavelength [Å]	0.931	0.9796	0.9495	1.006
		Data Statistics		
resolution [Å]	20.0−1.8	20.0−1.8	20.0−1.8	20.0−1.9
no. of observations total/unique	1838767/ 41485	224757/ 40676	197851/ 50595	155856/ 39886
completeness (total/high) [%][a]	99.7/ 99.8	98.9/ 95.0	97.4/ 99.0	98.8/ 96.0
$\langle I/\sigma(I)\rangle$ (total/high)[a]	19.5/ 4.4	19.1/ 3.5	12.3/ 4.1	15.0/ 3.3
R_{sym} (total, high)[a,b]	4.7/ 38.1	5.5/ 42.5	6.8/ 32.4	4.9/ 33.4
		Refinement Statistics		
refinement program	CNS	Refmac	CNS	CNS
resolution range [Å]	20−1.9	10.0−1.8	20.0−1.75	20.0−1.9
included amino acids	10−414	10−414	10−414	10−414
residues in region of Ramachandran plot [%]				
allowed	90.0	90.0	88.5	88.8
additional allowed	10.0	9.7	11.5	11.2
generously allowed	0.0	0.3	0.0	0.0
disallowed	0.0	0.0	0.0	0.0
no. of protein atoms	3207	3215	3253	3210
no. of water molecules	412	415	384	521
no. of ligand atoms	43 (heme), 11 (Cam)	43 (heme), 11 (Cam), 2 (CN)	43 (heme), 11 (Cam)	43 (heme), 11 (Cam), 2 (CN)
no. of metal ions	2	2	2	2
R_{work}, R_{free} [%][c]	21.9/26.4	17.6/22.0	19.62/22.3	18.9/23.5
rms dev bonds/angles [Å/deg]	0.006/1.64	0.014/1.55	0.007/1.32	0.009/1.35
Wilson *B*-factor [Å^2]	29.7	30.1	30.4	35.9
$\langle B\rangle$ (all atoms/heme/Cam/CN/waters) [Å^2]	23.7/18.4/19.5/—/29.8	23.0/15.6/23.8/21.2/35.8	25.2/16.2/25.6/—/35.0	32.0/26.2/36.2/32.9/40.3
B-factor [Å] and occupancy of active site water molecules	n.a.	Wat901: 32.2/0.7 Wat902: 24.3/1.0	n.a.	Wat901: 0.0/0.0 Wat902: 42.2/1.0
coordinates error by Luzzati plot [Å]	0.24	0.19	0.20	0.24

[a] Completeness, R_{sym} and $\langle I/\sigma(I)\rangle$ are given for all data and for the highest resolution shell: P450_G248T_ferric, 1.9−1.8 Å; P450_G248T_CN, 1.9−1.8 Å; P450_G248V_ferric, 1.85−1.75 Å; P450_G248V_CN, 2.0−1.9 Å. [b] $R_{sym} = \sum|I - \langle I\rangle|/\sum I$. [c] $R_{work} = \sum||F_{obs}| - k|F_{calc}||/\sum|F_{obs}|$. 5% of randomly chosen reflections were used for the calculation of R_{free}.

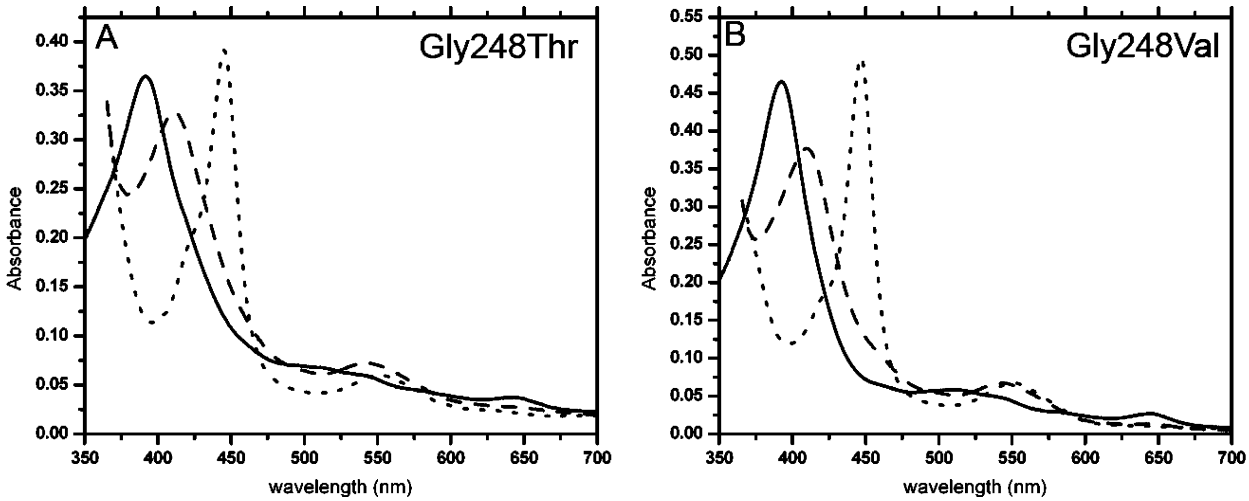

FIGURE 2: Optical charaterization of the Gly248Thr (left) and Gly248Val (right) mutant P450s in the ferric camphor bound (solid), ferrous deoxy (dashed) and ferrous carbonmonoxy (dotted) states.

bond scission (*16*, *17*, *20*). The Gly248 mutants additionally resemble the phenotype of mutants at the conserved threonine position in that they are increasingly more uncoupled as a function of active-site dehydration (*7*, *8*, *36*). Given that this minimization of uncoupling in the reaction of CYP101 with non-native substrates has been optimized by reducing the degree of hydration of the P450 active site (*5*, *37*, *38*), this result was somewhat surprising, and indicates that there is indeed a fine-tuning of the type and degree of active-site water to maintain "coupled" P450 metabolism. In order to ensure that the observed uncoupling of electron consumption to hydroxycamphor formation was not simply attributable

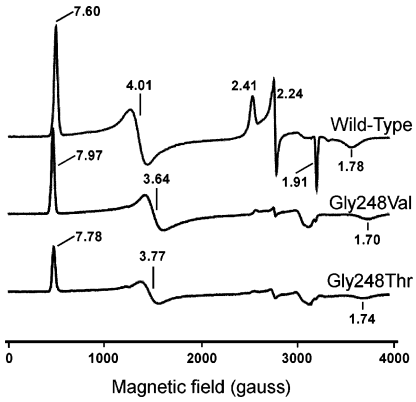

FIGURE 3: X-band EPR of the ferric camphor bound WT and Gly248Thr and Val mutants.

Table 2: Summary of EPR Parameters of Camphor Bound WT and Gly248 Mutants

	EPR g-values	
protein	high-spin	low-spin
Gly248 (WT)	7.60, 4.01, 1.78	2.41, 2.24, 1.95
Gly248Thr	7.78, 3.77, 1.74	2.38, 2.22, 1.92
Gly248Val	7.97, 3.64, 1.70	2.37, 2.23, 1.96

Table 3: Steady-State Kinetic Parameters of Gly248 CYP101 Mutants

	Gly248	Gly248Thr	Gly248Val
NADH oxidation (nmol/min/nmol P450)	834 ± 16	194 ± 14	64 ± 6
product formation (nmol/min/nmol P450)	820 ± 32	146 ± 8	18 ± 1
coupling (%)	98 ± 5	75 ± 9	28 ± 4
autoxidation (min^{-1}) ($\times$10000)	5.8 ± 0.3	3.9 ± 0.3	3.7 ± 0.3

to autodecay of the ferrous−dioxygen complex to produce superoxide, the autoxidation rates of the Gly248 mutants were measured and compared to that of the wild-type enzyme (Table 3). The autoxidation rates of both 248Val and 248Thr closely resemble that of the wild-type enzyme. In comparison, in the Thr252Ala mutant, a 10-fold increase of this process has been observed (*8*), which has implicated the role of the threonine hydroxyl in stabilizing the oxyferrous intermediate in CYP101. In the case of both Thr252Ala and the Gly248Val and Thr mutants, the observed uncoupling to peroxide formation likely indicates a perturbation of second proton delivery (to the hydroperoxo complex) resulting from alterations of the hydrogen-bonding interactions in the distal pocket (*10*, *14*).

Kinetic Solvent Isotope Effects (KSIE)

Kinetic solvent isotope effects have been utilized as a useful probe of proton delivery in a number of enzymatic reactions, including the oxygen activation processes of cytochrome P450 (*20*, *39*) and other monooxygenases (*40*). As isotopic substitution has previously been shown to exclusively affect P450 catalysis at second electron transfer, and subsequent proton-transfer processes involved in producing the high-valent oxoferryl intermediate (*39*), the impact on rate ratio can provide an important indication of the number and identity of protons in the active site during O−O bond heterolysis (*20*). In agreement with previous reports

Table 4: Solvent-Isotope Effect Measurements of NADH Oxidation and Product Formation of Wild-Type P450 and Gly248 Mutants

	k_{H2O}/k_{D2O}	
	NADH oxidation	product formation
wild-type[a]	1.5 ± 0.15	1.66 ± 0.18
Gly248Thr	0.81 ± 0.06	1.37 ± 0.07
Gly248Val	0.79 ± 0.07	1.19 ± 0.07

Table 5: Coupling Efficiencies of 5-Hydroxycamphor Formation to Electron Consumption in Protic and Deuterium Solvents

	nmol of product/nmol of NADH consumed		
	H_2O	D_2O	H_2O/D_2O
wild-type	0.98 ± 0.03	0.89 ± 0.03	1.10
Gly248Thr	0.74 ± 0.02	0.63 ± 0.02	1.17
Gly248Val	0.28 ± 0.04	0.16 ± 0.02	1.75

on CYP101, a significant solvent isotope effect is observed in the rate constants for electron consumption and turnover for the wild-type enzyme (Table 4). However, upon introduction of the larger side chains of the Gly248Thr and Gly248Val mutants in the active site, the overall magnitude of the solvent isotope effect decreases and even reaches a negative effect in terms of electron consumption. In comparison, in previous studies of the Asp251Asn mutant, in which electron consumption decreases by roughly 3 orders of magnitude, the solvent isotope effect exhibits a drastic increase ($k_H/k_D \sim 6$ at a p*L* of 7), which was rationalized structurally and chemically as an increase of the number of protons "in flight" as a result of distal pocket opening through disruption of salt bridges at the I-helix (*20*). At the simplest level, one may expect that the occlusion of active-site water may be expected to indeed elicit the opposite scenario, which would manifest itself in a reduction of the number of protons in flight in the rate-limiting step of the reaction, namely, second electron transfer and subsequent proton transfer.

In order to more carefully assess the role of solvent and exchangeable protons on the parameters of electron consumption and monooxygenation coupling, the effective coupling of NADH to product formation was examined in H_2O and D_2O (Table 5). Through the use of the 248 mutant series, which are fractionally uncoupled to varying degrees, the involvement of proton transfer on the branchpoint of monooxygenation and peroxide formation can be more thoroughly evaluated. Like the steady-state kinetic parameters, there is an increase of P450 uncoupling in deuterium solvents, which becomes more pronounced as the Gly248 side chain substitution becomes larger. In the case of 248Val, coupling to monooxygenation is almost twice as effective in protic versus deuterium containing solvent. This illustrates that the rate constants of the proton-transfer reactions that govern the branchpoint of monooxygenation and uncoupling parameters are not only highly sensitive to the hydration of the distal pocket but must also become at least partially rate limiting in the P450 cycle, otherwise no effect could be expected. A more detailed mechanistic interpretation of the isotopic effect on coupling ratios is presented in the discussion.

EPR Characterization of Peroxoferric Intermediates

In order to generate an additional, and in some ways more direct, assessment of the efficacy of proton transfer in the

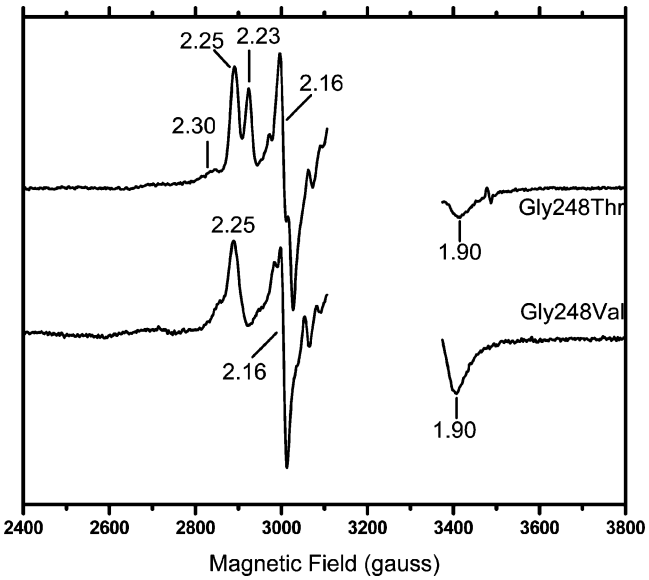

FIGURE 4: X-band EPR of the 77 K cryoradiolytically reduced oxyGly248Thr and Val CYP101 enzymes.

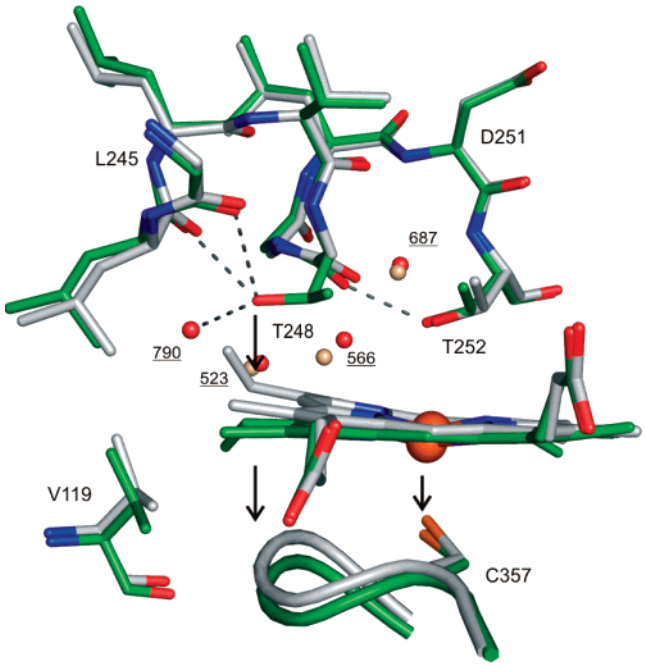

FIGURE 5: Overlaid structures of the wild type (1dz4, gray) and Gly248Thr mutant (green) CYP101 in the ferric-camphor bound state (camphor not shown). The bulkier side chain of Thr248 induces the planarization of the heme in the mutant enzyme, which is followed by the repositioning of the heme binding loop and some surrounding residues like Val119. The Thr248 hydroxyl group is hydrogen bonding to preceding residues in the I-helix and a new water molecule (790), leading to slight deviations in the conformation of the distal pocket residues. The unusual H-bond between the carbonyl oxygen atom of Thr248 and the hydroxyl group of Thr252 is maintained.

mutant P450 cytochromes, we have generated the peroxoferric intermediates via cryoradiolysis of the precursor ferrous−dioxygen complexes. As oxyferrous P450 represents the last kinetically isolatable intermediate in the P450 reaction cycle (*4*, *41*), this constitutes the only current method by which to specifically probe the efficacy of proton transfer following reduction of this intermediate. Earlier EPR and ^{1}H electron nuclear double resonance (ENDOR) studies (*10*, *11*) have indicated that alterations of proton delivery may be monitored by characteristic changes of the **g**-tensor (or coupled proton signal in ENDOR studies) which are sensitive to protonation at the distal oxygen, and can additionally be evaluated by their respective annealing temperature dependences. In the case of wild-type P450 CYP101 (and heme oxygenase), a native proton delivery network enables facile transfer of this proton at temperatures below 77 K, whereas in the well-characterized Asp251Asn mutant of CYP101, higher-temperature annealing (>170 K) is necessary. Therefore, the EPR characterization of the primary cryoreduced product at 77 K can serve as an effective method to assess the 248 mutants for their ability to effectively mediate proton transfer. The cryoreduction of oxyGly248Thr and oxyGly248Val (Figure 4) results in an EPR signal similar to that of the Asp251Asn mutant of P450 CYP101 (*10*, *11*), with *g* values of 2.24, 2.16, and 1.94 that are diagnostic of the unprotonated peroxoanion species with end-on geometry of the dioxygen ligand, as opposed to a hydroperoxo−ferric species (WT and Thr252Ala), which has a characteristically larger *g*-spread, as monitored by the change in this g_1-value from $g \sim 2.24$ to $g \sim 2.30$ (*10*, *11*). In the cryogenically prepared Gly248Thr peroxoanion intermediate, an additional low-spin species ($g_1 \sim 2.23$) is observed, which has also been observed in studies of the analogous intermediate in both camphor bound Asp251Asn (*42*) and methylenecamphor bound Thr252Ala (*43*), and most likely represents a distinct conformer of the peroxoanion (or precursor oxyferrous) species. The reason for the absence of this conformer in the identically prepared intermediate in Gly248Val is unclear. It may reflect a decreased mobility of the dioxygen ligand since the valine side chain which is not fixed in its conformation by hydrogen bonding like the threonine side chain (see below) may occupy a larger volume in the distal pocket.

The EPR spectra of peroxoanion adducts of both 248Thr and 248Val additionally indicate that, despite the introduction of either threonine or valine residues at the 248 position, the peroxo complexes most likely retain a normal geometry in terms of Fe−OO bond angle. This conclusion is also supported by the crystallographic characterization of ferricyanide adducts described below. A "perturbed" geometry of the hydroperoxo ligand, such as that seen in cryoradiolytically generated peroxo-heme oxygenase, is often characterized by an abnormally large g_1 value, in which a decrease of the Fe−OO bond angle in the peroxo complex has been correlated to its function in mediating direct heme hydroxylation by a peroxo adduct (*14*). This is not observed in either the Gly248Thr or Gly248Val mutant. Therefore, analogous to the Asp251Asn mutant of CYP101, cryoradiolysis studies support that the observed rate of product formation (and electron consumption) is due to impairment of proton delivery to the peroxo−anion intermediate.

X-ray Crystallographic Studies

Gly248Thr. Upon mutation of Gly248 to threonine, several distinct structural changes take place in the active site of the enzyme. Most obviously, the bulkier side chain of the threonine residue requires more space than the native glycine (Figure 5). To prevent a steric clash, the vinyl group of the C pyrrole ring rotates toward the heme plane, resulting in a

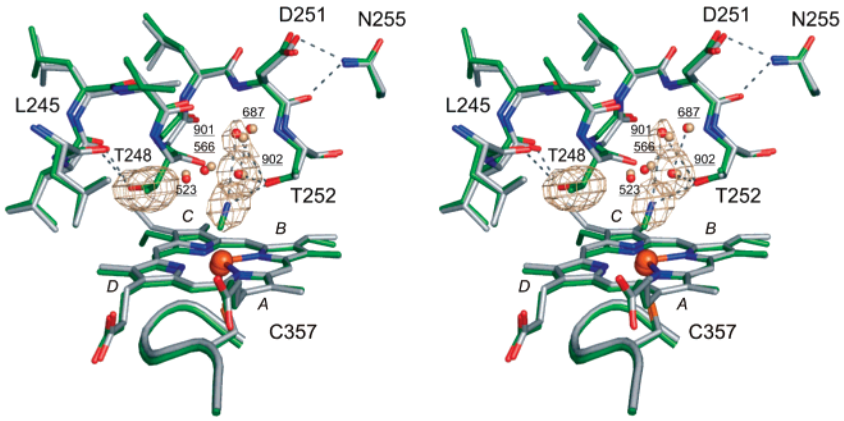

FIGURE 6: Stereoview of the superposed cyano complexes of wildtype (1o76, gray) and Gly248Thr CYP101 (green). Letters in italics denote the heme pyrrole rings. There is difference electron density in the mutant enzyme (initial $F_o - F_c$ map, contoured at 3σ) for both of the catalytic water molecules. However, Wat901 is less occupied or more mobile than Wat902.

Table 6: Calculated Out-of Plane Distortions in Various Derivatives of Wild-Type, Gly248Val, and Gly248Thr CYP101 Based on NSD Analysis

P450	PDB	state	D_{oop}[a] (Å)	B_{2u} (Å)	B_{1u} (Å)	A_{2u} (Å)	ref (Å)
WT	1PHC	Fe^{3+} substrate-free	0.54	0.15	0.36	0.22	(*59*)
	1DZ4	Fe^{3+} substrate-bound	0.53	0.31	0.43	0.03	(*19*)
	1DZ6	Fe^{2+}	0.48	0.24	0.40	0.03	(*19*)
	1DZ8	$Fe^{2+}-O_2$	0.40	0.27	0.27	0.01	(*19*)
	1DZ9	$Fe^{4+}-O$	0.32	0.20	0.21	0.06	(*19*)
G248T		Fe^{3+} substrate-bound	0.15	0.04	0.02	0.13	this work
		$Fe^{3+}-CN$	0.29	0.13	0.24	0.06	this work
G248V		Fe^{3+} substrate-bound	0.30	0.03	0.03	0.18	this work
		$Fe^{3+}-CN$	0.21	0.11	0.14	0.08	this work

[a] Total out-of-plane heme distortion.

small change in the positions of Val119 and Leu362, and, more importantly, a movement of the C and D pyrrole rings which results in a flattening of the heme (see Figure 6 and Table 6 for normal mode analysis of the heme geometry). In comparison to the wild-type enzyme, changes of the heme comprise displacements of 0.8 Å of the carbon atom C3C and 0.6 Å of C2C in ring C to 0.4−0.5 Å of atoms C2D and C3D in ring D, and of 0.3 Å of the heme iron. Accordingly, the region of the L-helix (residues 357−366) adjacent to the axial cysteine follows suit and is also shifted up to 0.7 Å. The side chain of the inserted threonine 248 is oriented toward the I-helix, where its hydroxyl group forms hydrogen bonds with the carbonyl oxygen atoms of Leu244 (3.1 Å) and Leu245 (3.0 Å), respectively, and with a newly occurring water molecule (Wat790, 3.0 Å) located beyond this helix. This interaction results in a 0.2 to 0.4 Å shift of the peptide backbone of residues 242 to 254. This movement causes a displacement of the water molecules located in the oxygen binding niche (Wat523 0.6 Å, Wat566 0.9 Å). Despite this, the unusual hydrogen bond between the hydroxyl group of the active site Thr252 and the carbonyl oxygen of residue 248 is maintained.

The new water molecule Wat790 is located near Phe163 in the E-helix (3.6 Å). This region lines a hydrophobic cavity formed by the I-helix (Leu 245 and Leu246), the C-helix (Val118 and Val119), and which has been found to bind xenon and was therefore proposed to serve as an oxygen storage site ((*44*), pdb code 1uyu). In the xenon bound state, the phenyl ring of Phe163 is pushed upward (Δ0.3 Å) with respect to the heme plane by Xe1421 located 3.2 Å away from its CE1 atom, creating one of two possible side-chain conformations of this residue. Wat790 is located at the opposite site of the ring, between the I-helix and Phe163, and seems to exert the same effect, potentially together with minor contributions from the side chains of Leu245, Leu246 and Val119, which are oriented slightly differently than in the wild-type enzyme.

To assess the changes induced by oxygen binding, we determined the structure of the stable cyanide complex (shown in Figure 6) since it has been shown to be a good structural oxygen mimic (*26*). At the sixth ligand position, electron density for an end-on (η1) bound cyanide molecule is clearly observed, showing a similar binding geometry as in the wild-type enzyme (Fe−C bond length 1.9 Å, Fe−C−N angle 149°). Compared to the ferric form of the mutant, the heme adopts a more ruffled conformation. This, together with the movement of the iron into the heme plane by 0.4 Å, results in changes of the conformation of the loop containing Cys357, Leu348 (located beneath pyrrole ring D), and Gly359. As in the wild-type cyano complex, cyanide points toward Thr252 which rotates to form a hydrogen bond (3.1 Å) with the distal nitrogen atom. This results in a widening of the groove formed by the stretch of residues encompassing Thr248 to Thr252. In addition, the Thr252 backbone amide flips toward the active site, thereby changing its position by 0.6 Å. This, and the rotation of the Thr252 side chain, results in the binding of two new water molecules, which were originally observed in the oxy complex of the wild-type enzyme (*19*). In analogy, these water molecules were dubbed Wat901 and Wat902. Even though one cannot refine occupancy and *B*-factors independently at a resolution of 1.9 Å, it is apparent that Wat901 is either rather mobile or not fully occupied. Nevertheless, the presence of Wat901 and Wat902 induces shifts of Wat566 and Wat523 by 1.0 Å and 0.5 Å, respectively. Due to the bulk of the Thr248 side chain, the changes in the I-helix are not restricted to the widening of the oxygen binding niche, but extend toward Met241.

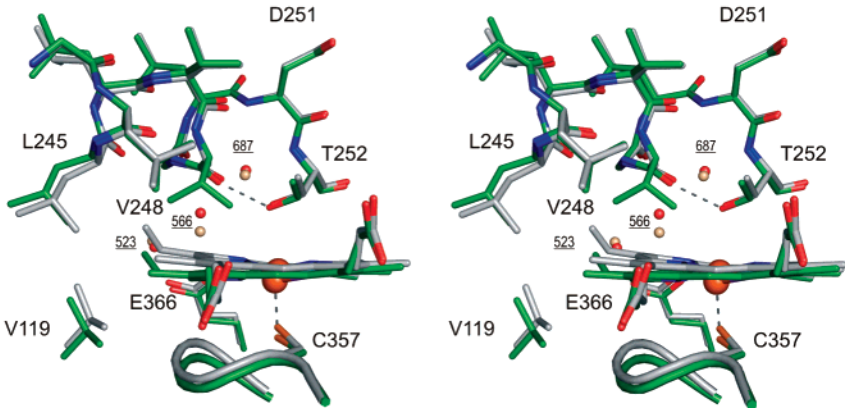

FIGURE 7: Structural comparison of wild type (1dz4, gray) and Gly248Val (green) CYP101 in the ferric state. The changes in the structure of the active site induced by Val248 are similar to the ones observed in the Gly248Thr mutant except for the orientation of the valine side chain.

A structural comparison of the cyanide complexes of the Gly248Thr mutant and the wild-type enzyme (pdb code 1o76, molecule A), respectively, shows that the main differences occur in the heme geometry, which is less ruffled in the mutant enzyme, the conformation of the oxygen binding niche, and a network of water molecules in the distal pocket that connects to Glu366. The change in water structure is caused by a sterically induced rearrangement of the carbonyl group of Leu245 to prevent a tight interaction with the hydroxyl group of Thr248. Gly249 follows in order to preserve the hydrogen bond between its backbone amide and the carbonyl of Leu245 (2.8 Å), which results in a widening of the groove in the I-helix. This affects the positions of the carbonyl group of Thr248 and of the amide group of Thr252, and thereby the interacting Wat902 (Δ0.2 Å) and Wat901 (Δ0.4 Å), respectively. These water molecules are considered to be essential for proton delivery during catalysis (*20*, *45*).

Gly248Val. In the ferric state, the Gly248Val enzyme closely resembles the threonine mutant as the side chain of Val248 is oriented very similarly. However, unlike the hydroxyl group of the threonine in the other mutant, the methyl groups on the Cβ atom point toward the heme binding pocket since they are not involved in hydrogen bonding with the I-helix but may form interactions with the aromatic π-electron system of the heme. Since the similar steric dimensions of the valine side chain would also lead to a steric clash with the vinyl group on the C ring of the heme, the vinyl group is shifted downward and rotated away from this residue. An analogous downward movement of the heme rings C and D takes place (e.g., C3C (0.9 Å), C4C (1.0 Å), C2C and C2D (0.6 Å)) which flattens the heme and subsequently induces the displacement of surrounding residues like Val119 and the L-helix around Cys357 by up to 0.7 Å (Figure 7). The larger side chain also affects the conformation of the backbone from residues 249 to 243 in the I-helix as judged by the deviations in the C-alpha trace when overlaid with the wild type. In particular, the carbonyl oxygen of residue 248 changes its position by 0.3 Å and adopts a slightly different angle. This and the slight change in the position of Glu366 seem to induce a change in the water structure in the oxygen binding cavity such that Wat566 can favorably interact with the carbonyl group of Val248. Wat566 moves closer by 0.9 Å to a distance of 3.7 Å, whereas Wat523 and Wat687 move by 0.3 Å. Although there is no additional water molecule located behind the I-helix like in the Gly248Thr mutant (Wat790), residue Phe163 appears to be shifted by 0.4 Å. The cause for this is not apparent, since the side chains of Leu245, Leu246 and Val119 adopt slightly different conformations than in the wild type. These changes could be sufficient to induce a repositioning of this residue.

To assess the structural changes induced by binding of a sixth ligand, the structure of the cyanide complex was determined (Figure 8) and compared with the corresponding structure of the wild-type enzyme (*26*) and of the Gly248Thr mutant, described above. The structures of the two mutants are very similar, with the exception that Wat901 is missing. The immediate reason is not obvious from the structure alone.

DISCUSSION

Active-site hydrogen bonding plays an important role in the dioxygen activation process in the P450 cytochromes, and has been extensively investigated in a number of CYPs in addition to CYP101. In CYPs that do not contain the active-site threonine (e.g., CYP107A1 and CYP158A2), it has been speculated that hydroxyl groups from the substrate itself may play a role in establishing the hydrogen-bonding network required to promote effective monooxygenation (*46*−*48*). The results presented herein support the notion that the extensively studied conserved acid−alcohol is not the sole determinant in establishing the catalytic efficiency of the P450 monooxygenation reaction, and that active-site hydration is highly important in governing its efficacy. The kinetic and spectroscopic results indicate that changes in the number and timely availability of water molecules in the P450 distal pocket likely perturb proton delivery at both stages. This is manifested both in a reduction of turnover and electron consumption rates, and the coupling of reducing equivalents to hydroxylated product. In contrast, mutagenesis of the conserved active-site acid and alcohol results in perturbations of first and second proton delivery exclusively. The radiolytic reduction of the oxyferrous complex in Gly248Val or Thr results in exclusive production of a peroxoanion species at 77 K. This demonstrates that the first proton required for heterolysis is not effectively transferred in either of the mutants, similar to the observation in the Asp251Asn mutant.

In support of these findings, Wat901 is missing entirely in the X-ray structure of the Gly248Val mutant (as in

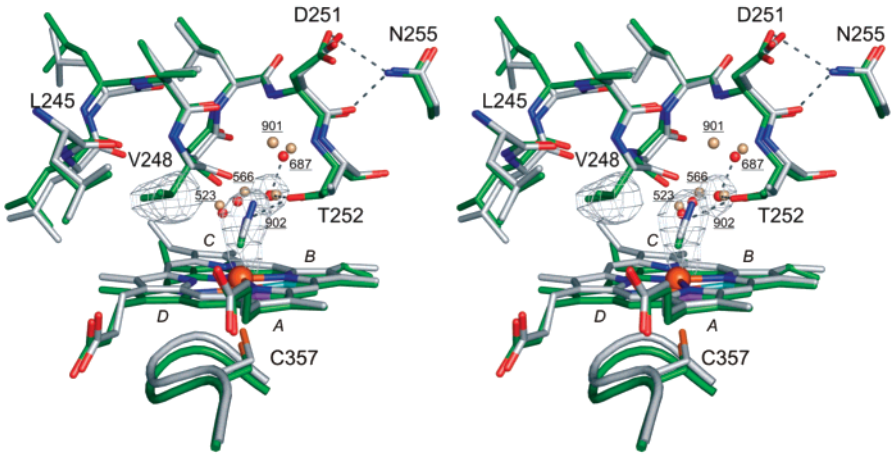

FIGURE 8: Stereoview of the structural superposition of wildtype (1o76, gray) and Gly248Val CYP101 (green) in the cyanide-bound state. In this mutant, electron density was only detectable for the catalytic water molecule Wat902, although the backbone carbonyl oxygen atom of Asp251 is flipped. The initial $F_o - F_c$ electron density map (contoured at 3σ) for Wat902, the cyanide ligand and the Val248 side chain is shown.

Asp251Asn) whereas it has a lower occupancy or higher mobility in the Gly248Thr mutant. Based on the following considerations, the complete or partial absence of Wat901 is thought to be mechanistically significant. In the cyanide complex of the wild-type enzyme (*26*), both Wat901 and Wat902 are fully occupied. Their *B*-factors as a measure of their mobility appear to be very similar to each other in both of the molecules, that are contained in the asymmetric unit (molecule A, both 28 Å^2; molecule B, 22 Å^2 for Wat 901, 18 Å^2 for Wat 902), and close to the Wilson *B*-factor of the structure (27 Å^2). In comparison, in the structure of the Gly248Thr mutant, which was determined at the same resolution as wild-type (1.8 Å), the intensity for Wat901 in a $F_o - F_c$ electron density map was weaker than for Wat902. On the basis of the electron density, its occupancy was estimated to be 0.7. Since the *B*-factors and the occupancy cannot be refined independently at this resolution, this resulted in a *B*-factor value of 32 Å^2, which is similar to the *B*-factor of Wat902 (24 Å^2) and the overall Wilson *B*-factor (30 Å^2). In the Gly248Val mutant, no electron density could be observed for Wat901 in the $F_o - F_c$ electron density map. In contrast, Wat902 is fully occupied. The resolution of the data of the Gly288Val mutant is slightly lower (1.9 Å) and its Wilson *B*-factor (36 Å^2) slightly higher. Correspondingly, the *B*-factor of Wat902 (42 Å^2) as well as the average *B*-factor for all ordered water molecules (40 Å^2) is higher than in the Gly248Thr structure. However, given the observation from both the wild-type and the Gly248Thr structures, that the *B*-factors for Wat901 and Wat902 are in the same range, this cannot solely account for the missing electron density of Wat901. It seems highly likely that the introduction of a bulky amino acid residue in close proximity to the cyanide binding site leads to a perturbation of the water structure in the active site, especially since the gradual decrease in the product formation rates of the two mutant proteins (Gly248Thr > Gly248Val) is mirrored in the occupancy of Wat901.

The use of mutants which are fractionally coupled to different degrees has additionally elucidated the importance of solvent and exchangeable groups in determining the fate of peroxo complexes after initial protonation to form the branching hydroperoxo intermediate. Earlier annealing experiments of the hydroperoxoferric species in CYP101 in the presence of substrate analogues have shown the dramatic role that substrate identity has on the reactivity of these states (*43*, *49*), in agreement with previous studies which have shown metabolic switching (i.e., the change of the ultimate fate of active intermediates) upon substrate deuteration (*50*, *51*) or halogenation (*6*). Under the increasingly uncoupled conditions employed in the mutants described here, the kinetic solvent isotope effect on substrate turnover decreases significantly (and approaches unity), while the rate of NADH consumption modestly increases, resulting in a net increase of uncoupling in D_2O versus H_2O when compared to the wild-type enzyme. As a result, this data can be viewed on the basis of the comparative rates of productive proton transfer (those resulting in heterolytic cleavage to compound I) versus uncoupling, and therefore reflect an important measure of the intrinsic lifetime of the branching intermediate. Previous low temperature annealing experiments of the uncoupled Thr252Ala peroxo complex (*10*) and the Asp251Asn/Thr252Ala double mutant (unpublished data), in which direct decay of the hydroperoxo complex to the ferriheme resting state is observed, strongly indicate this as the branching intermediate. As the overall rate of proton transfer involved in O−O heterolysis slows, deuterium substitution would be expected to have a greater influence on the coupling ratio, given the assumption that the release of hydrogen peroxide is a proton-independent process and represents dissociation of the relatively weak hydroperoxo ligand from the enzyme. Therefore, solvent isotopic substitution in the 248 mutant series, in which proton delivery is hampered, would be expected to have a greater impact on the coupling efficiencies than in the wild-type enzyme if the intrinsic rate of hydroperoxo ligand dissociation does not change significantly across the mutant series. As the autoxidation rate of the oxyferrous complex may provide an indication for the propensity of oxygen ligand dissociation as a result of changes in the active-site hydrogen-bonding patterns, one may infer that hydroperoxo ligand dissociation may similarly not be altered significantly in the mutants, and could even be stabilized in the increasingly apolar environment as observed in model studies (*52*, *53*).

A similar dependence of solvent isotope dependence on resulting product stoichiometry has been observed in CYP17, in which the observed alteration in heavy water was

interpreted as controlling the ratio of oxene versus peroxide catalyzed hydroxylation and side-chain cleavage reactivities respectively (*54*). Analogously, the effect of solvent exchange on coupling parameters was also extensively addressed in the mononuclear iron enzyme putidamonooxin with substrates of ranging coupling efficiencies (*55*). In this case, however, both an increase of product formation and coupling efficiency was observed in D_2O relative to H_2O, with suppression of H_2O_2 (or D_2O_2) formation, an effect which was observed to instead decrease as a more "uncoupled" substrate was used. These results are consistent in that the influence of active-site proton-transfer pathways (as governed by exchangeable groups) is critical in the determination of active-intermediate transformation, and that the observed effect of solvent on fractional coupling and decoupling reflects the difference of the intrinsic mechanisms of the enzymes mentioned above, which can putatively utilize an oxo or peroxo intermediate (CYP17), a peroxo intermediate (putidamonooxin), and solely the oxo intermediate (CYP101 camphor hydroxylation). Recent results by Klinman and colleagues have additionally implicated that the transfer of a "prebound oxygen" to the heme iron in part controls the $k_{cat}/K_m(O_2)$ in CYP101 (*56*). The results in the 248Thr and 248Val mutants, which would structurally be expected to limit oxygen binding by blocking steric access to the heme iron, may, in addition to inhibiting proton-transfer subsequent to reduction of the oxyferrous complex, be expected to hinder this process as well. As a result, one would expect that the observed kinetic solvent isotope effect on hydroxylation rates would increasingly reflect this oxygen binding step, which has been established earlier as being isotopically insensitive (*39*). While our present studies cannot rigorously address this possibility, the observed changes of coupling parameters as a function of isotopic substitution (and mutation) suggest that proton transfer significantly contributes to the slow and uncoupled rates of product formation in the Gly248 series.

Structurally, the inefficiency of proton delivery in the mutants can be specifically linked to changes in the water structure of the distal pocket. An enhanced degree of dehydration, specifically, the low occupancy (G248Thr) or lack (G248Val) of Wat901 (observed in the oxyferrous (*19*) and cyanide bound (*26*) wild-type CYP101), can be correlated to a reduction of the efficacy of first proton transfer to form the hydroperoxo species. This observation is in agreement with structural studies of the Asp251Asn oxyferrous complex, in which this water molecule is missing, entirely. However, we cannot exclude the possibility that the efficiency of first proton transfer may additionally relate to the ability of Asp251Asn to flip down toward the active site as suggested in QM/MM studies (*57*) and therefore provide a distal charge relay system as previously suggested (*17*), a movement which is certain to be inhibited in the Gly248Val and Thr mutants. However, this conformational flexibility has not been observed crystallographically in P450.

The reduction of coupling efficiency, and hence the ability to deliver the second proton required for monooxygenation, is more difficult to structurally assess. The Thr252 hydroxyl undergoes very subtle structural changes upon mutation of the Gly248 residue. Additionally, the autoxidation rates of the mutants are not accelerated as in the Thr252Ala mutant, and in fact are slightly slower than that of the wild-type enzyme. However, these studies do indicate that the threonine hydroxyl itself is not the key determinant in establishing coupling efficiency as a direct proton donor, in line with extensive mutagenesis studies which indicate that the ability of the 252 side chain to accept a hydrogen bond is the most important physicochemical property necessary to maintain coupling efficiency (*58*). This has recently been extended by Nagano et al., from analysis of the oxyferrous structures of the Thr252Ala mutant, in a proposal that the main role of the threonine hydroxyl is to serve as a hydrogen bond acceptor to the hydroperoxy species, thereby increasing the proton affinity of the distal oxygen to promote heterolysis (*18*). However, a closer comparison between the structures of the oxy complexes of the wild type and Thr252Ala protein shows that Wat901 is moved by ~0.6 Å and that this change is transmitted in displacements of the other water molecules resulting in the net loss of one water molecule; Wat567 moved to take up the position of Wat902. This change in active site water structure is in line with our results which indicate that it is indeed the distal pocket solvent structure (as determined in part by the threonine hydroxyl in WT CYP101) that not only dictates the efficacy of primary proton transfer to the peroxoanion complex but also determines the fate of the hydroperoxo complex to either form a high-valent species or produce hydrogen peroxide. Thus, while the threonine hydroxyl is clearly important in maintaining the hydrogen-bonding pattern of the distal pocket, and in particular the associated solvent structure, it does not solely determine the coupling efficiency in the P450 cytochromes following reduction of the oxyferrous complex. Given the vast range of active-site volumes observed in CYPs and their corresponding active-site flexibility, and the associated coupling values (often very low), the role of solvation is likely a key determinant in catalytic efficiency of many of these enzymes.

A rather unanticipated result of these studies is the drastic changes in heme geometry observed upon distal pocket rearrangement, which can be observed both spectroscopically and structurally. A comparison of heme geometry parameters of CYP101 enzymes in the ferric and cyano states is listed in Table 6, as determined from the normal-coordinate structural decomposition method developed by Shelnutt and coworkers (*60*). In the case of both the high-spin and low-spin hexacoordinate states, the total out of plane distortion of the heme macrocycle dramatically reduces upon introduction of the distal pocket mutant. The planarity of the porphyrin macrocycle may be expected to alter various parameters of heme-catalysis, including ligand binding, redox potential, and axial ligand affinity. A change in thiolate binding geometry is not observed in the Gly248Val and Thr structures, as a coordinated movement of thiolate accompanies the change in heme geometry, resulting in negligible net changes in Fe−SCys bond length. However, the increase of heme planarity may be expected to additionally alter other parameters in catalysis, and would be expected to stabilize the reduced form in the enzyme, resulting in faster rates of primary electron transfer (the subject of future investigation) and have contributions in enhancing oxyferrous stability (Table 3).

In conclusion, the investigation of mutants at the P450 distal pocket reveals that maintaining the number and location of active-site water molecules is important for effective proton mediated oxygen activation in CYPs. The maintenance of a correct degree and pattern of active-site hydration

is critical for mediating the efficient transfer of both the first and second protons of catalysis, leading to efficient heterolytic scission. These results present the mechanistic importance of active-site water in evaluating active-site hydrogen bonding in other CYPs, other heme and non-heme dioxygen activating enzymes, and may additionally aid in the redesign of P450s to efficiently metabolize alternative substrates.

ACKNOWLEDGMENT

We gratefully appreciate the help provided by Dr. John Bentley while using the ^{60}Co source in the Notre Dame Radiation Laboratory (Notre Dame University, IN) and the support by the X10SA beamline staff at the Swiss Light Source, Paul Scherer Institute, Villigen, Switzerland. Irradiations were conducted at the Notre Dame Radiation Laboratory, which is a facility of the U.S. Department of Energy, Office of Basic Energy Sciences.

REFERENCES

1. Guengerich, F. P. (2001) Common and Uncommon Cytochrome P450 Reactions Related to Metabolism and Chemical Toxicity, *Chem. Res. Toxicol. 14*, 611−650.
2. Denisov, I. G., Makris, T. M., Sligar, S. G., and Schlichting, I. (2005) Structure and chemistry of cytochrome P 450, *Chem. Rev. 105*, 2253−2277.
3. Li, X., Baudry, J., Berenbaum, M. R., and Schuler, M. A. (2004) Structural and functional divergence of insect CYP6B proteins: from specialist to generalist cytochrome P450, *Proc. Natl. Acad. Sci. U.S.A. 101*, 2939−2944.
4. Brewer, C. B., and Peterson, J. A. (1986) Single turnover studies with oxy-cytochrome P 450cam, *Arch. Biochem. Biophys. 249*, 515−521.
5. Jones, N. E., England, P. A., Rouch, D. A., and Wong, L. L. (1996) Engineering the selectivity of aliphatic C-H bond oxidation catalysed by cytochrome P450cam, *Chem. Commun.* 2413−2414.
6. Kadkhodayan, S., Coulter, E. D., Maryniak, D. M., Bryson, T. A., and Dawson, J. H. (1995) Uncoupling Oxygen-Transfer and Electron-Transfer in the Oxygenation of Camphor Analogs By Cytochrome P450-Cam−Direct Observation of an Intermolecular Isotope Effect For Substrate C-H Activation, *J. Biol. Chem. 270*, 28042−28048.
7. Imai, M., Shimada, H., Watanabe, Y., Matsushima-Hibiya, Y., Makino, R., Koga, H., Horiuchi, T., and Ishimura, Y. (1989) Uncoupling of the cytochrome P-450cam monooxygenase reaction by a single mutation, threonine-252 to alanine or valine: possible role of the hydroxy amino acid in oxygen activation, *Proc. Natl. Acad. Sci. U.S.A. 86*, 7823−7827.
8. Martinis, S. A., Atkins, W. M., Stayton, P. S., and Sligar, S. G. (1989) A Conserved Residue of Cytochrome-P-450 Is Involved in Heme-Oxygen Stability and Activation, *J. Am. Chem. Soc. 111*, 9252−9253.
9. Sligar, S. G., Lipscomb, J. D., Debrunner, P. G., and Gunsalus, I. C. (1974) Superoxide anion production by the autoxidation of cytochrome P 450cam, *Biochem. Biophys. Res. Commun. 61*, 290−296.
10. Davydov, R., Makris, T. M., Kofman, V., Werst, D. E., Sligar, S. G., and Hoffman, B. M. (2001) Hydroxylation of camphor by reduced oxy-cytochrome P450cam: Mechanistic implications of EPR and ENDOR studies of catalytic intermediates in native and mutant enzymes, *J. Am. Chem. Soc. 123*, 1403−1415.
11. Davydov, R., Macdonald, I. D. G., Makris, T. M., Sligar, S. G., and Hoffman, B. M. (1999) EPR and ENDOR of catalytic intermediates in cryoreduced native and mutant oxy-cytochromes P450cam: Mutation-induced changes in the proton delivery system, *J. Am. Chem. Soc. 121*, 10654−10655.
12. Poulos, T. L., Finzel, B. C., Gunsalus, I. C., Wagner, G. C., and Kraut, J. (1985) The 2.6-Å crystal structure of Pseudomonas putida cytochrome P-450, *J. Biol. Chem. 260*, 16122−16130.
13. Denisov, I. G., Makris, T. M., and Sligar, S. G. (2002) Formation and decay of hydroperoxo-ferric heme complex in horseradish peroxidase studied by cryoradiolysis, *J. Biol. Chem. 277*, 42706−42710.
14. Davydov, R. M., Yoshida, T., Ikeda-Saito, M., and Hoffman, B. M. (1999) Hydroperoxy-Heme Oxygenase Generated by Cryoreduction Catalyzes the Formation of α-meso-Hydroxyheme as Detected by EPR and ENDOR, *J. Am. Chem. Soc. 121*, 10656−10657.
15. Raag, R., Martinis, S. A., Sligar, S. G., and Poulos, T. L. (1991) Crystal-Structure of the Cytochrome-P-450cam Active-Site Mutant Thr252ala, *Biochemistry 30*, 11420−11429.
16. Gerber, N. C., and Sligar, S. G. (1994) A role for Asp-251 in cytochrome P-450cam oxygen activation, *J. Biol. Chem. 269*, 4260−4266.
17. Gerber, N. C., and Sligar, S. G. (1992) Catalytic mechanism of cytochrome P-450: evidence for a distal charge relay, *J. Am. Chem. Soc. 114*, 8742−8743.
18. Nagano, S., and Poulos Thomas, L. (2005) Crystallographic study on the dioxygen complex of wild-type and mutant cytochrome P450cam. Implications for the dioxygen activation mechanism, *J. Biol. Chem. 280*, 31659−31663.
19. Schlichting, I., Berendzen, J., Chu, K., Stock, A. M., Maves, S. A., Benson, D. E., Sweet, R. M., Ringe, D., Petsko, G. A., and Sligar, S. G. (2000) The catalytic pathway of cytochrome p450cam at atomic resolution, *Science 287*, 1615−1622.
20. Vidakovic, M., Sligar, S. G., Li, H., and Poulos, T. L. (1998) Understanding the role of the essential Asp251 in cytochrome p450cam using site-directed mutagenesis, crystallography, and kinetic solvent isotope effect, *Biochemistry 37*, 9211−9219.
21. LeBrun, L. A., Xu, F., Kroetz, D. L., and Ortiz de Montellano, P. R. (2002) Covalent attachment of the heme prosthetic group in the CYP4F cytochrome P450 family, *Biochemistry 41*, 5931−5937.
22. LeBrun, L. A., Hoch, U., and Ortiz De Montellano, P. R. (2002) Autocatalytic mechanism and consequences of covalent heme attachment in the cytochrome P450 4A family, *J. Biol. Chem. 277*, 12755−12761.
23. Henne, K. R., Kunze, K. L., Zheng, Y.-M., Christmas, P., Soberman, R. J., and Rettie, A. E. (2001) Covalent Linkage of Prosthetic Heme to CYP4 Family P450 Enzymes, *Biochemistry 40*, 12925−12931.
24. Limburg, J., LeBrun, L. A., and Ortiz de Montellano, P. R. (2005) The P450cam G248E Mutant Covalently Binds Its Prosthetic Heme Group, *Biochemistry 44*, 4091−4099.
25. Seward, H. E., Girvan, H. M., and Munro, A. W. (2005) Cytochrome P450s: creating novel ligand sets, *Dalton Trans.* 3419−3426.
26. Fedorov, R., Ghosh, D. K., and Schlichting, I. (2003) Crystal structures of cyanide complexes of P450cam and the oxygenase domain of inducible nitric oxide synthase−structural models of the short-lived oxygen complexes, *Arch. Biochem. Biophys. 409*, 25−31.
27. Kabsch, W. (1993) Automatic Processing of Rotation Diffraction Data from Crystals of Initially Unknown Symmetry and Cell Constants, *J. Appl. Crystallogr. 26*, 795−800.
28. Brunger, A. T., Adams, P. D., Clore, G. M., DeLano, W. L., Gros, P., Grosse-Kunstleve, R. W., Jiang, J.-S., Kuszewski, J., Nilges, M., Pannu, N. S., Read, R. J., Rice, L. M., Simonson, T., and Warren, G. L. (1998) Crystallography & NMR System: a new software suite for macromolecular structure determination, *Acta Crystallogr., Sect. D: Biol. Crystallogr. 54*, 905−921.
29. Murshudov, G. N., Vagin, A. A., Lebedev, A., Wilson, K. S., and Dodson, E. J. (1999) Efficient anisotropic refinement of macromolecular structures using FFT, *Acta Crystallogr., Sect. D: Biol. Crystallogr. 55* (Part 1), 247−255.
30. DeLano, W. L. (2002) The Pymol Molecular Graphics System, DeLano Scientific, San Carlos, CA.
31. Bailey, S. (1994) The CCP4 suite: programs for protein crystallography, *Acta Crystallogr ., Sect. D: Biol. Crystallogr. 50*, 760−763.
32. Lipscomb, J. D. (1980) Electron Paramagnetic Resonance Detectable States of Cytochrome P450cam, *Biochemistry 19*, 3590−3599.
33. Tsai, R. L., Yu, C.-A., Gunsalus, I. C., Peisach, J., Blumberg, W., Orme-Johnson, W. H., and Beinert, H. (1970) Spin-state changes in cytochrome P-450cam on binding of specific substrates, *Proc. Natl. Acad. Sci. U.S.A. 66*, 1157−1163.
34. LeLean, J. E., Moon, N., Dunham, W. R., and Coon, M. J. (2000) EPR spectrometry of cytochrome P4502B4: Effects of mutations and substrate binding, *Biochem. Biophys. Res. Commun. 276*, 762−766.

35. Cosper, N. J., Scott, R. A., Hori, H., Nishino, T., and Iwasaki, T. (2001) X-ray absorption spectroscopic analysis of the high-spin ferriheme site in substrate-bound neuronal nitric-oxide synthase, *J. Biochem. (Tokyo) 130*, 191−198.
36. Shimada, H., Watanabe, Y., Imai, M., Makino, R., Koga, H., Horiuchi, T., and Ishimura, Y. (1991) The Role of Threonine 252 in the Oxygen Activation by Cytochrome P-450cam: Mechanistic Studies by Site-directed Mutagenesis, in *Dioxygen Activation and Homogeneous Catalytic Oxidation* (Simandi., L. I., Ed.), pp 313−319, Elsevier Science Publishers, B. V., Amsterdam.
37. Loida, P. J., and Sligar, S. G. (1993) Molecular Recognition in Cytochrome-P-450 - Mechanism For the Control of Uncoupling Reactions, *Biochemistry 32*, 11530−11538.
38. Loida, P. J., and Sligar, S. G. (1993) Engineering cytochrome P-450cam to increase the stereospecificity and coupling of aliphatic hydroxylation, *Protein Eng. 6*, 207−212.
39. Aikens, J., and Sligar, S. G. (1994) Kinetic Solvent Isotope Effects During Oxygen Activation By Cytochrome P-450cam, *J. Am. Chem. Soc. 116*, 1143−1144.
40. Lee, S.-K., and Lipscomb, J. D. (1999) Oxygen Activation Catalyzed by Methane Monooxygenase Hydroxylase Component: Proton Delivery during the O-O Bond Cleavage Steps, *Biochemistry 38*, 4423−4432.
41. Eisenstein, L., Debey, P., and Douzou, P. (1977) P 450cam: oxygenated complexes stabilized at low temperature, *Biochem. Biophys. Res. Commun. 77*, 1377−1383.
42. Makris, T. M. (2004) Ph.D. Thesis, University of Illinois, Urbana, IL.
43. Davydov, R., Perera, R., Jin, S., Yang, T.-C., Bryson, T. A., Sono, M., Dawson, J. H., and Hoffman, B. M. (2005) Substrate modulation of the properties and reactivity of the oxy-ferrous and hydroperoxo-ferric intermediates of cytochrome P450cam as shown by cryoreduction-EPR/ENDOR spectroscopy, *J. Am. Chem. Soc. 127*, 1403−1413.
44. Wade, R. C., Winn, P. J., Schlichting, I., and Sudarko, A. (2004) survey of active site access channels in cytochromes P450, *J. Inorg. Biochem. 98*, 1175−1182.
45. Benson, D. E., Suslick, K. S., and Sligar, S. G. (1997) Reduced oxy intermediate observed in D251N cytochrome P450(cam), *Biochemistry 36*, 5104−5107.
46. Nagano, S., Cupp-Vickery, J. R., and Poulos, T. L. (2005) Crystal Structures of the Ferrous Dioxygen Complex of Wild-type Cytochrome P450eryF and Its Mutants, A245S and A245T: Investigation of the proton transfer system in P450eryF, *J. Biol. Chem. 280*, 22102−22107.
47. Cupp-Vickery, J. R., Han, O., Hutchinson, R., and Poulos, T. L. (1996) Substrate-assisted catalysis in cytochrome P450eryF, *Nat. Struct. Biol. 3*, 632−637.
48. Zhao, B., Guengerich, F. P., Voehler, M., and Waterman, M. R. (2005) Role of Active Site Water Molecules and Substrate Hydroxyl Groups in Oxygen Activation by Cytochrome P450 158A2: A new mechanism of proton transfer, *J. Biol. Chem. 280*, 42188−42197.
49. Kim, S. H., Yang, T.-C., Perera, R., Jin, S., Bryson, T. A., Sono, M., Davydov, R., Dawson, J. H., and Hoffman, B. M. (2005) Cryoreduction EPR and 13C, 19F ENDOR study of substrate-bound substates and solvent kinetic isotope effects in the catalytic cycle of cytochrome P450cam and its T252A mutant, *Dalton Trans.* 3464−3469.
50. Atkins, W. M., and Sligar, S. G. (1988) Deuterium isotope effects in norcamphor metabolism by cytochrome P-450cam: kinetic evidence for the two-electron reduction of a high-valent iron-oxo intermediate, *Biochemistry 27*, 1610−1616.
51. Atkins, W. M., and Sligar, S. G. (1987) Metabolic switching in cyctochrome P-450cam: deuterium isotope effects on regiospecificity and the monooxygenase/oxidase ratio, *J. Am. Chem. Soc. 109*, 3754−3760.
52. Roelfes, G., Vrajmasu, V., Chen, K., Ho, R. Y. N., Rohde, J.-U., Zondervan, C., la Crois, R. M., Schudde, E. P., Lutz, M., Spek, A. L., Hage, R., Feringa, B. L., Muenck, E., and Que, L., Jr. (2003) End-On and Side-On Peroxo Derivatives of Non-Heme Iron Complexes with Pentadentate Ligands: Models for Putative Intermediates in Biological Iron/Dioxygen Chemistry, *Inorg. Chem. 42*, 2639−2653.
53. Ho, R. Y. N., Roelfes, G., Hermant, R., Hage, R., Feringa, B. L., and Que, L., Jr. (1999) Resonance Raman evidence for the interconversion between an $[Fe^{III}$-η^1-OOH$]^{2+}$ and $[Fe^{III}$-η^2−$O_2]^+$ species and mechanistic implications thereof, *Chem. Commun. 21*, 2161−2162.
54. Swinney, D. C., and Mak, A. Y. (1994) Androgen Formation by Cytochrome P450 CYP17. Solvent Isotope Effect and pL Studies Suggest a Role for Protons in the Regulation of Oxene versus Peroxide Chemistry, *Biochemistry 33*, 2185−2190.
55. Twilfer, H., Sandfort, G., and Bernhardt, F. H. (2000) Substrate and solvent isotope effects on the fate of the active oxygen species in substrate-modulated reactions of putidamonooxin, *Eur. J. Biochem. 267*, 5926−5934.
56. Purdy, M. M., Koo, L. S., Ortiz de Montellano, P. R., and Klinman, J. P. (2006) Mechanism of O2 Activation by Cytochrome P450cam Studied by Isotope Effects and Transient State Kinetics, *Biochemistry 45*, 15793−15806.
57. Taraphder, S., Hummer, G. (2003) Protein Side-Chain Motion and Hydration in Proton-Transfer Pathways. Results for Cytochrome P450cam, *J. Am. Chem. Soc. 125*, 3931−3940.
58. Kimata, Y., Shimada, H., Hirose, T., and Ishimura, Y. (1995) Role of Thr-252 in Cytochrome P450(Cam)—a Study With Unnatural Amino-Acid Mutagenesis, *Biochem. Biophys. Res. Commun. 208*, 96−102.
59. Poulos, T. L., Finzel, B. C., and Howard, A. J. (1986) Crystal structure of substrate-free Pseudomonas putida cytochrome P-450, *Biochemistry 25*, 5314−5322.
60. Jentzen, W., Ma, J.-G., and Shelnutt, J. A. (1998) Conservation of the Conformation of the Porphyrin Macrocycle in Hemoproteins *Biophys. J. 74*, 753−763.

BI7013695